Materials Science & Engineering A 777 (2020) 139022

Contents lists available at ScienceDirect

Materials Science & Engineering A

journal homepage: http://www.elsevier.com/locate/msea

Short communication

Growth kinetics, microhardness and microstructure evolution of undercooled FeCoNiCuSn high entropy alloy

M.R. Rahul, Gandham Phanikumar *

Department of Metallurgical and Materials Engineering, Indian Institute of Technology Madras, Chennai, 600036, India

ARTICLE INFO

Keywords:
Undercooling
High entropy alloy
Growth kinetics
Solute addition

ABSTRACT

Multi-principle element alloy FeCoNiCu with varying Sn addition was undercooled using the meltfluxing technique to illustrate the dependence of growth kinetics on Sn addition. The alloy $FeCoNiCuSn_{0.5}$ shows morphological variation in the microstructure from dendritic to equiaxed grain morphology with the increase in undercooling. The alloy $FeCoNiCuSn_5$ shows dendrite morphology with undercooling. The dendritic growth velocity was sluggish with solute addition,i.e., at an undercooling of 200 K, the growth velocity decreased from ~25 m/s to 6 m/s while varying Sn concentration from 0.5 to 5 at % suggesting solute drag effect. The microhardness improvement could be correlated to the microstructure refinement achieved during undercooling.

1. Introduction

Multi principle element alloys– often referred to as high entropy alloys or complex concentrated alloys – have gained attention in recent times due to their remarkable properties [1]. Some of these alloys have exhibited improved mechanical properties than their commercially established alternatives making them attractive for future applications [2–4]. Studies on microstructure stability in this class of alloys show a strong dependence on the processing route adopted for the synthesis of these alloys [5]. The single phase solid solution formation in these alloys is attributed to several core effects that includes sluggish diffusion [6]. However, recent reports show that solute diffusion cannot be assumed to be sluggish because of the increase in configurational entropy [7,8]. The tracer diffusion reports in FeCoNiCrMn system suggest that diffusion behaviour depends upon the type of atoms in the alloy [7]. There are no studies on the effect of solute on the growth kinetics during solidification in this class of alloys.

In melt processing routes a faster cooling rate or solidification rate usually involves a deeper undercooling of the melt. Studies on solidification microstructure using undercooling as a control parameter provide insights into the phase selection and formation of metastable microstructures [9,10]. Measurement of the speed of recalescence front during solidification is often used to quantify the growth kinetics in undercooled alloys. The high speed video analysis was used in various research groups to quantify the growth kinetics and thereby understand the material behaviour at undercooled condition [11]. The studies on Fe–Co system shows that the imaging techniques are able to capture the double recalescence event in the system as well as the growth kinetics measured can be used to verify the current dendritic growth theories [12]. The growth kinetics with *in situ* observation was reported for intermetallic compounds like Ni–Zr system shows lower growth velocity [13]. The growth velocity calculated from *in situ* measurements can give idea about the mechanism of growth which is reported in Ni–Zr system where dendritic growth is changed to a coupled growth [14]. The reports on Fe-based alloys and Ni-based alloys suggest that solute addition plays a vital role in the growth kinetics of the alloys in undercooled condition [15,16]. In Fe-based alloys, Co addition was shown to increase the growth velocity, whereas Si addition decreases the growth velocity [15]. Fe based multicomponent alloy shows the use of rapid solidification by giving undercooling for improving the microhardness by grain refinement and also the reports suggest the decrease in growth velocity with addition of solute in Fe [17]. Decrease in velocity was observed in Fe–Cu system compared with pure iron due to the addition of Cu [18]. The effect of Cu addition on Ni and stress induced recrystallization were reported in Ni–Cu system [19]. Analytical prediction have shown that small amount of impurity will increase the growth velocity at lower undercooling regime [20]. The growth velocity calculations on Ni-based alloys show that the increase in Zr addition will slow down the growth kinetics [16]. While there are studies on elemental segregation during solidification of high entropy alloys that form a single phase, there are no studies that document solute drag effect in these alloys.

There are only a few studies that present growth kinetics of HEAs in

* Corresponding author.
E-mail address: gphani@iitm.ac.in (G. Phanikumar).

https://doi.org/10.1016/j.msea.2020.139022
Received 30 August 2019; Received in revised form 22 January 2020; Accepted 27 January 2020
Available online 8 February 2020

undercooled condition [21,22], but those do not use *in situ* observations of recalescence front motion similar to the ones on conventional alloys and functional materials [10,23]. Deep undercooling was shown to have a significant effect on the microstructure and properties of alloys. The increased hardness in Fe-based alloy due to undercooling was prominent compared to solid solution strengthening [15]. Morphological variation with respect to undercooling was reported in Fe-Ni [24] and Cu–Ni alloys [25]. Liquid phase separation was observed in undercooled or high cooling rate condition in Co-Cu [26,27] and Fe–Cu [18] binary alloys. In this study, we have chosen the alloy $FeCoNiCuSn_x$ to study the effect of solute addition by comparing alloys containing Sn of 0.5 and 5 atomic percentages.

2. Experimental details

The alloys are prepared from high purity elements (99.9%) in required proportions and melted using vacuum arc melting technique. The homogeneity of the button sample was ensured by melting 6 times and flipping each time. Samples for metallography and undercooling were taken from the button using electrical discharge machining. The

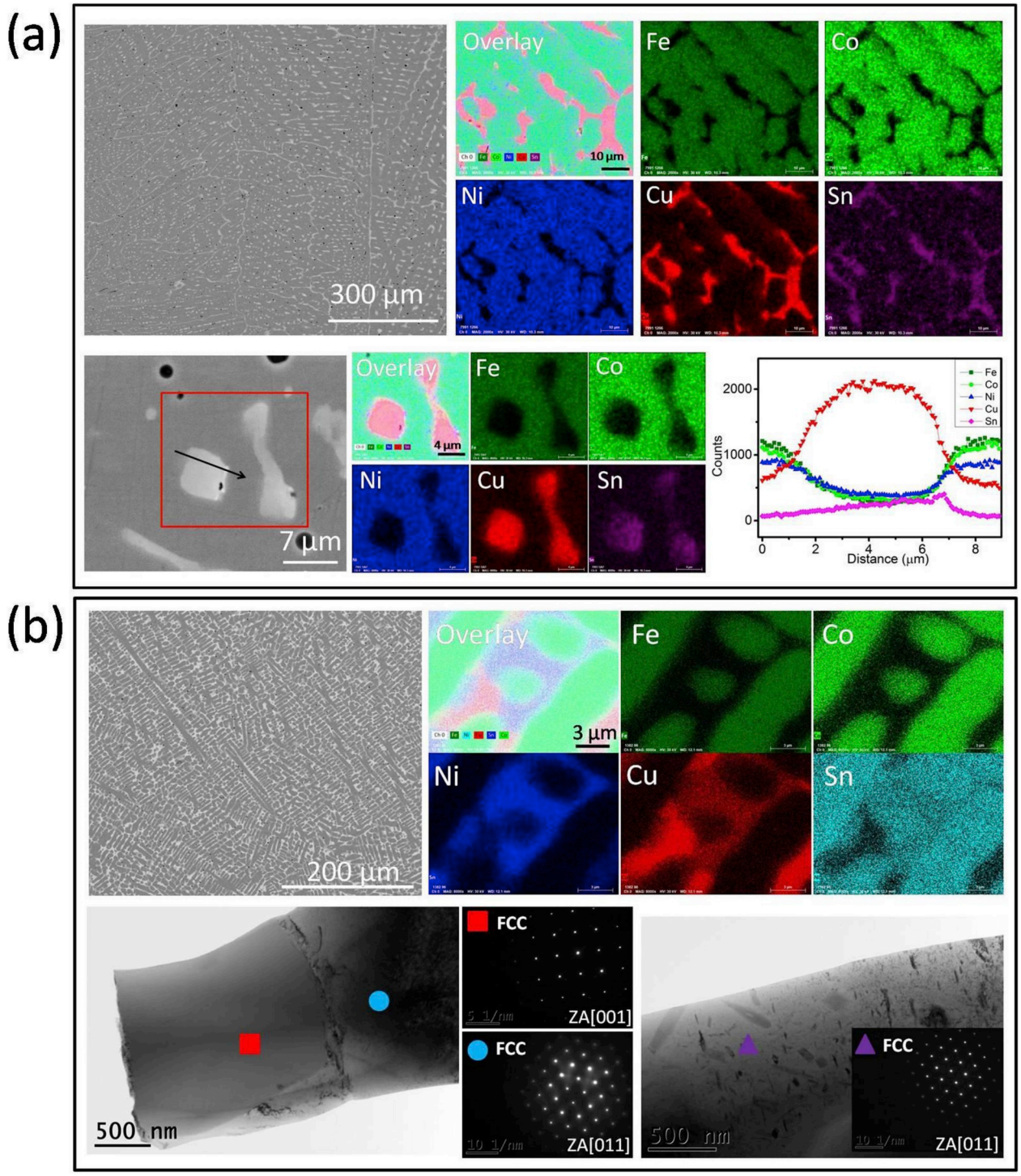

Fig. 1. a) BSE- SEM images, EDS elemental mapping and line scan at interdendritic region of as-cast $FeCoNiCuSn_{0.5}$, b) BSE-SEM image, EDS elemental mapping and Phase identification using TEM of as cast $FeCoNiCuSn_5$ as-cast alloy.

sample was placed in a boron trioxide flux, and the undercooling experiment was carried out in Argon atmosphere. The *in situ* thermal profile was captured using a two-colour pyrometer. The speed of recalescence front motion during solidification of the undercooled sample was captured by using high-speed video imaging operating at 10^5 frames per second. The thermal contrast was adequate to record the recalescence front motion. The microstructures of as-cast and undercooled samples were taken using scanning electron microscopy in back-scattered electron mode. The compositional analysis was carried out using energy dispersive spectroscopy, and elemental maps were collected for elemental distribution between phases. The as-cast $FeCoNiCuSn_5$ sample was characterised using transmission electron microscopy with EDS attachment to confirm the phases. Independently, the phases of the as-cast and undercooled samples were also identified by XRD (presented in supplementary file, Fig. S3). The hardness variation with respect to undercooling was studied using microhardness testing with a force of 500 gf and a dwell time of 10 s.

3. Results and discussion

Fig. 1a shows the as-cast microstructure of $FeCoNiCuSn_{0.5}$ alloy consisting primary dendritic phase with interdendritic segregation. The nominal and measured composition of as-cast sample is shown in Table 1. The EDS mapping confirms that the primary phase was enriched with the Fe, Co and Ni, and the interdendritic region is enriched with Cu. The compositions of the primary phase and interdendritic region are listed in Table 2. The structure was confirmed as FCC from the XRD measurements (supplementary file, Fig. S3). This could be attributed to the negative enthalpy of mixing of Fe with Co and Ni as well as zero enthalpy of mixing between Co–Ni. The large positive enthalpy of mixing of Cu with Fe, Co, Ni could explain the segregation in the interdendritic region [28]. Sn is segregated in between the Cu rich interdendritic region, and FeCoNi rich primary phase as confirmed by the EDS mapping and the corresponding line scan. This is expected from the positive enthalpy of mixing of Sn with Fe, Co, and Cu. Fig. 1b shows the as-cast microstructure of $FeCoNiCuSn_5$ alloy; SEM BSE image shows a primary dendritic phase with the interdendritic region. The EDS mapping confirms that the primary phase is enriched with Fe, Co, Ni and the interdendritic region consists of two phases – one rich in Cu–Ni–Sn and the other rich in Cu. The TEM micrograph with SAED pattern confirms that the three phases are of FCC structure. Table 2 shows the composition of different phases taken from EDS.

Microstructure evolution $FeCoNiCuSn_{0.5}$ alloy with respect to undercooling is shown in Fig. 2a. At lower undercooling regime ($\Delta T < 74$ K) the microstructure shows dendritic morphology with interdendritic region enriched with Cu and Sn segregation. Columnar dendritic morphology was observed at an undercooling range of $74 < \Delta T < 111$ K and distorted dendritic morphology was observed between 111 K to 177 K. At higher undercooling regime ($\Delta T > 200$ K) the sample shows equiaxed grain morphology, which can be confirmed by the Cu segregated surrounding the Fe–Co–Ni rich phase. The equiaxed grain morphology is similar to what is reported in Ni–Cu alloy, where it was attributed to recrystallization [29]. Microstructure evolution of undercooled $FeCoNiCuSn_5$ was shown in Fig. 2b where the dendrite morphology was observed in the entire undercooling regime studied here. The Cu–Ni–Sn rich phase and Cu rich phases are present in the all level of undercooling. The EDS analysis in each phase (supplementary file, Fig. S6) confirms that the composition in FeCoNi rich primary phase and Cu–Ni–Sn rich phase have similar values in all levels of undercooling. The Cu rich phase shows decrease in Cu amount at highest undercooling while increase in Fe, Co, Ni amounts in interdendritic region may attribute to the trapping of Cu in the primary phase. Solute trapping was observed in $FeCoNiCuSn_{0.5}$ which can be confirmed by the increase in Cu amount in FeCoNi rich primary phase with respect to increase in undercooling (supplementary file, Fig. S7). The microstructure was refined at the higher undercooling, and the XRD results (supplementary file, Fig. S3) confirm that there is no formation of any additional phase in these samples. The deconvoluted XRD peak shows the three phases formed with a close lattice parameter.

Growth velocity was determined as a function of undercooling by tracking the recalescence front motion in the undercooled sample. The recalescence front was seen to be of angular morphology at the lower undercooling and spherical morphology at higher undercooling regime (supplementary file, Fig. S4). Such a variation was also reported in undercooled Nickel [30]. The growth velocity variation with respect to undercooling for the currently studied alloys is shown in Fig. 3. The growth rate is higher at deeper undercooling within the range of undercooling explored in this study. The growth rates were significantly different for the two alloys suggesting that solute addition plays an essential role in the growth kinetics of these alloys. The plot of growth rate illustrates that the velocity was sluggish when Sn addition was increased from 0.5 to 5 at %. At undercooling of 200 K, the growth velocity of ~25 m/s was observed in $FeCoNiCuSn_{0.5}$ alloy whereas it was only ~6 m/s for $FeCoNiCuSn_5$ alloy. We believe that this decrease in growth velocity can be attributed to the solute drag effect. The $FeCoNiCuSn_{0.5}$ alloy shows the maximum velocity of ~65 m/s at an undercooling of 270 K, which is comparable to Fe or Ni-based alloys or pure metals. A minute addition of boron in Ni showed the same effect where the velocity drastically decreased with increase in boron content [31]. This high velocity in higher undercooling domain suggests that the alloy behaves like dilute alloys where the growth kinetics is fast unlike what is expected from the presence of multiple principal elements in the alloy.

The growth velocity data was fit using an exponential function $V = A \exp(B\Delta T)$ where A will depends on solute concentration, and diffusion and B will depend on the heat generation due to dendrite formation [15]. The bulk undercooling obtained in the sample consists of contributions from solutal undercooling, curvature undercooling, kinetic undercooling and thermal undercooling [32]. Studies on most metallic alloys have shown that at low undercooling regime, the contribution from solutal and curvature undercooling is dominant as the growth is diffusion controlled. At higher undercooling, the thermal and kinetic undercooling is dominant as the growth is typically collision controlled. The data in this study were fit to a high value for the constant A for $FeCoNiCuSn_{0.5}$ alloy ($A = 3.146$) compared to $FeCoNiCuSn_5$ ($A = 1.328 \times 10^{-5}$) alloy. This high value of A shows that the effect of solutal undercooling is dominant in the $FeCoNiCuSn_{0.5}$ compared to the

Table 1
Composition of as-cast alloys.

Elements	$FeCoNiCuSn_5$		$FeCoNiCuSn_{0.5}$	
	Nominal composition (at %)	Measured composition (at %)	Nominal composition (at %)	Measured composition (at %)
Fe	23.75	26.36 ± 0.11	24.875	27.5 ± 0.15
Co	23.75	25.03 ± 0.11	24.875	26.06 ± 0.15
Ni	23.75	22.86 ± 0.05	24.875	23.73 ± 0.11
Cu	23.75	21.33 ± 0.15	24.875	22.23 ± 0.40
Sn	5	4.4 ± 0.05	0.5	0.43 ± 0.05

Table 2
Composition of phases (in atomic percentage) of as-cast sample using EDS analysis.

Elements	$FeCoNiCuSn_5$			$FeCoNiCuSn_{0.5}$	
	FeCoNi rich phase	Cu rich phase	CuNiSn rich phase	FeCoNi rich phase	Cu rich phase
Fe	31.41	5.83	5.00	27.88	6.63
Co	32.29	6.45	6.31	28.62	7.13
Ni	23.66	10.5	23.61	24.67	11.45
Cu	11.79	69.65	43.27	18.71	71.23
Sn	0.85	7.56	21.81	0.12	3.57

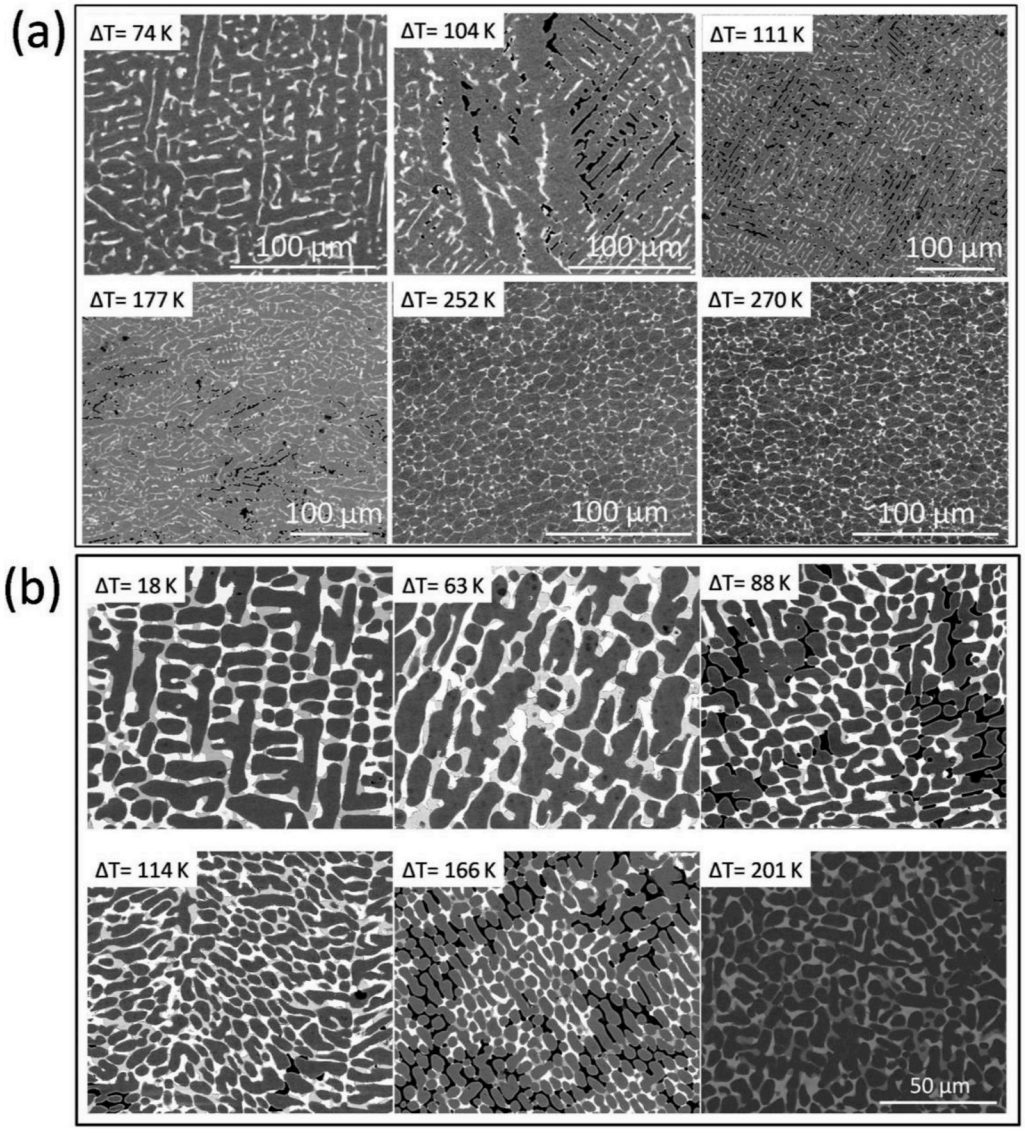

Fig. 2. a) Microstructure variation of undercooled $FeCoNiCuSn_{0.5}$ sample with respect to undercooling shows morphological variation from dendrite to columnar dendrite and equaxied grains, b) Microstructure variation of undercooled $FeCoNiCuSn_5$ sample with respect to undercooling shows stable dendritic morphology even in higher undercooling (Black colour shows the porosities or shrinkage defects generated during solidification).

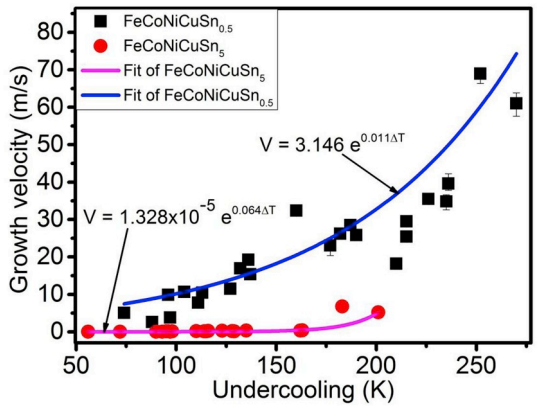

Fig. 3. Growth velocity variation of undercooled alloys with respect to undercooling where the continuous line shows the exponential fit and symbols show the experimental data points.

$FeCoNiCuSn_5$ alloy. The constant B is of the same order of magnitude for both alloys which further indicates that the driving force for solidification is more significant at $FeCoNiCuSn_5$ because of the comparatively high B value, but still, its growth velocity is sluggish.

The increase in growth velocity leads to refinement in the microstructure, which could lead to an improvement in mechanical property such as microhardness. Fig. 4a shows the microhardness variation of alloys in as-cast and undercooled condition. The microhardness was taken such a way that the values obtained are due to the contribution of multiple phases. Since all the phases in the $FeCoNiCuSn_5$ system are of FCC structure large deviation between the phases are not expecting which is accounted with multiple readings and the corresponding error bar provided. The increasing trend with respect to undercooling was observed in both cases. The $FeCoNiCuSn_{0.5}$ hardness was increased approximately to a maximum of 21% of the as-cast sample, which is due to the refinement of microstructure. Fig. 4b shows the secondary dendritic arm spacing, which confirms that secondary dendritic arm spacing decreases with respect to undercooling, and can explain the increase in the hardness through the Hall-Petch relationship. The hardness of as-cast $FeCoNiCuSn_5$ alloy was increased by 20% of as-cast

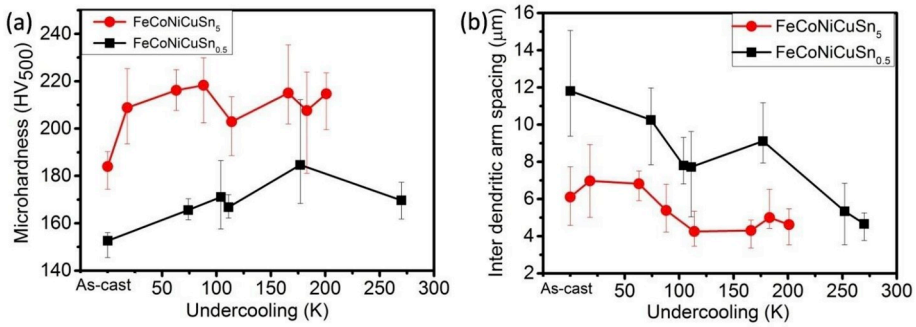

Fig. 4. a) Microhardess variation with respect undercooling for the studied alloys, b) inter dendritic arm spacing with respect to undercooling for the studied alloys (Here the as-cast sample value shows as the first data point).

$FeCoNiCuSn_{0.5}$ alloy mainly attributed to the solid solution strengthening as well as the presence of multiple phases. The hardness of the $FeCoNiCuSn_5$ alloy increased 19% of the as-cast alloy mainly attributed due to microstructure refinement. The microhardness of $FeCoNiCuSn_5$ alloy increased by 33% compared to $FeCoNiCuSn_{0.5}$ alloy at an undercooling of ~75 K. This is possibly due to the combined effect of solid solution strengthening and microstructure refinement due to undercooling.

This study shows that addition of Sn rather than Cu leads to the solute drag effect. This is verified by comparing with the growth velocity measurements of FeCoNiCu system (supplementary file, Fig. S5) which confirms that even 0.5 at % addition of Sn slows down the kinetics. From the literature, it is known that the elements that have a low equilibrium partition coefficient (ke«1) will promote the solute drag effect. This can be explained by the loss of driving force due to the solute drag as per Equation (1) [31,33].

$$\Delta G_d^L = \frac{RT(X^{L0} - X^{Li})^2}{2X^{L0}} \quad (1)$$

here, X^{Lo} is the initial composition of the parent phase, X^{Li} is the composition of liquid phase near to interface, T is the temperature, and R is the universal gas constant. Equation (1) shows that the decrease in free energy is proportional to (X^{Lo}- X^{Li}), which is larger in case of systems having low partition coefficient. In this system, Sn has a low value of partition coefficient compared to Cu so it will cause a reduction in the energy available for interface motion, which in turn reduce the growth kinetics. In the case of the Ni–B system, the growth velocity drastically reduced with increase in boron, which is characterised by a low value of partition coefficient [31]. The same effect can be observed in Ni–Zr system where an increase in Zr above 0.5 at% caused a reduction in growth kinetics due to solute drag effect [16]. In the $FeCoNiCuSn_{0.5}$ the partition coefficient of Sn (k_{sn}) is 0.033 whereas for Cu (k_{cu}) is 0.262, which is significantly larger than the partition coefficient of Sn. In $FeCoNiCuSn_5$ alloy the $k_{sn} = 0.038$ whereas $k_{cu} = 0.169$. In the Si–As system [34] solute drag effect was not observed and the partition coefficient in that system is large.

4. Conclusions

From this study, we propose that addition of Sn leads to solute drag effect and a decrease in the growth kinetics of undercooled $FeCoNiCuSn_x$. The microhardness improvement is attributed to the solid solution strengthening as well as the microstructure refinement due to undercooling. The morphological variations in the undercooled condition of $FeCoNiCuSn_{0.5}$ suggests that one can extend the concept of microstructure variation using undercooling from traditional alloys to the high entropy alloys too.

Data availability

The raw data required to reproduce these findings are available from the corresponding author on reasonable request.

Author contribution statement

All authors are equally contributed to this paper.

Originality statement

I write on behalf of myself and the co-author to confirm that the results reported in the manuscript are original and neither the entire work, nor any of its parts have been previously published. The authors confirm that the article has not been submitted to peer review, nor has been accepted for publishing in another journal. The author(s) confirms that the research in their work is original, and that all the data given in the article are real and authentic. If necessary, the article can be recalled, and errors corrected.

Declaration of competing interest

The authors declare that they have no known competing financial interests or personal relationships that could have appeared to influence the work reported in this paper.

Appendix A. Supplementary data

Supplementary data to this article can be found online at https://doi.org/10.1016/j.msea.2020.139022.

References

[1] D.B. Miracle, O.N. Senkov, A critical review of high entropy alloys and related concepts, Acta Mater. 122 (2017) 448–511, https://doi.org/10.1016/j.actamat.2016.08.081.
[2] Y.F. Ye, Q. Wang, J. Lu, C.T. Liu, Y. Yang, High-entropy alloy : challenges and prospects, Mater. Today 19 (2016) 349–362, https://doi.org/10.1016/j.mattod.2015.11.026.
[3] Z. Li, K.G. Pradeep, Y. Deng, D. Raabe, C.C. Tasan, Metastable high-entropy dual-phase alloys overcome the strength-ductility trade-off, Nature 534 (2016) 227–230, https://doi.org/10.1038/nature17981.
[4] Y.H. Jo, S. Jung, W.M. Choi, S.S. Sohn, H.S. Kim, B.J. Lee, et al., Cryogenic strength improvement by utilizing room-temperature deformation twinning in a partially recrystallized VCrMnFeCoNi high-entropy alloy, Nat. Commun. 8 (2017), 15719, https://doi.org/10.1038/ncomms15719, 1–8.
[5] F. He, Z. Wang, Y. Li, Q. Wu, J. Li, J. Wang, et al., Kinetic ways of tailoring phases in high entropy alloys, Sci. Rep. 6 (2016), 34628, https://doi.org/10.1038/srep34628, 1-8.
[6] B.S. Murty, J.W. Yeh, S. Ranganathan, P.P. Bhattacharjee, High Entropy Alloy, second ed., Elsevier, 2019.
[7] M. Vaidya, K.G. Pradeep, B.S. Murty, G. Wilde, S.V. Divinski, Bulk tracer diffusion in CoCrFeNi and CoCrFeMnNi high entropy alloys, Acta Mater. 146 (2018) 211–224, https://doi.org/10.1016/j.actamat.2017.12.052.

[8] M. Vaidya, S. Trubel, B.S. Murty, G. Wilde, S.V. Divinski, Ni tracer diffusion in CoCrFeNi and CoCrFeMnNi high entropy alloys, J. Alloys Compd. 688 (2016) 994–1001, https://doi.org/10.1016/j.jallcom.2016.07.239.
[9] K. Eckler, F. Gärtner, H. Assadi, A.F. Norman, A.L. Greer, D.M. Herlach, Phase selection, growth, and interface kinetics in undercooled Fe-Ni melt droplets, Mater. Sci. Eng. 226–228 (1997) 410–414, https://doi.org/10.1016/S0921-5093(96)10654-7.
[10] J. Gao, T. Volkmann, D.M. Herlach, Undercooling-dependent solidification behavior of levitated Nd14Fe79B7 alloy droplets, Acta Mater. 50 (2002) 3003–3012, https://doi.org/10.1016/S1359-6454(02)00128-3.
[11] J.W. Lum, D.M. Matson, M.C. Flemings, High-speed imaging and analysis of the solidification of undercooled nickel melts, Metall. Mater. Trans. B Process Metall. Mater. Process. Sci. 27 (1996) 865–870, https://doi.org/10.1007/BF02915616.
[12] J.E. Rodriguez, C. Kreischer, T. Volkmann, D.M. Matson, Solidification velocity of undercooled Fe-Co alloys, Acta Mater. 122 (2017) 431–437, https://doi.org/10.1016/j.actamat.2016.09.047.
[13] R. Kobold, W.W. Kuang, H. Wang, W. Hornfeck, M. Kolbe, D.M. Herlach, Dendrite growth velocity in the undercooled melt of glass forming Ni50Zr50 compound, Phil. Mag. Lett. 97 (2017) 249–256, https://doi.org/10.1080/09500839.2017.1330561.
[14] P. Lü, H.P. Wang, Observation of the transition from primary dendrites to coupled growth induced by undercooling within Ni-Zr hyperperitectic alloy, Scripta Mater. 137 (2017) 31–35, https://doi.org/10.1016/j.scriptamat.2017.05.006.
[15] Y. Ruan, S.Y. Chang, M. Dao, Comparative effect of rapid dendrite growth and element addition on microhardness enhancement of Fe-based alloys, Cryst. Growth Des. 15 (2015) 5661–5664, https://doi.org/10.1021/acs.cgd.5b01167.
[16] P.K. Galenko, G. Phanikumar, O. Funke, L. Chernova, S. Reutzel, M. Kolbe, et al., Dendritic solidification and fragmentation in undercooled Ni-Zr alloys, Mater. Sci. Eng. 449–451 (2007) 649–653, https://doi.org/10.1016/j.msea.2006.02.435.
[17] Y. Ruan, A. Mohajerani, M. Dao, Microstructural and mechanical-property manipulation through rapid dendrite growth and undercooling in an Fe-based multinary alloy, Sci. Rep. 6 (2016), 31684, https://doi.org/10.1038/srep31684, 1–11.
[18] S.B. Luo, W.L. Wang, J. Chang, Z.C. Xia, B. Wei, A comparative study of dendritic growth within undercooled liquid pure Fe and Fe50Cu50 alloy, Acta Mater. 69 (2014) 355–364, https://doi.org/10.1016/j.actamat.2013.12.009.
[19] X.L. Xu, Y.H. Zhao, H. Hou, The growth velocity-undercooling relationship of highly undercooled Ni and Ni-Cu melts, Mater. Sci. Technol. 35 (2019) 900–906, https://doi.org/10.1080/02670836.2019.1594553.
[20] O.V. Kazak, P.K. Galenko, D.V. Alexandrov, Influence of tiny amounts of impurity on dendritic growth in undercooled melts, IOP Conf. Ser. Mater. Sci. Eng. 192 (2017), 012030, https://doi.org/10.1088/1757-899X/192/1/012030.
[21] N. Liu, P.H. Wu, P.J. Zhou, Z. Peng, X.J. Wang, Y.P. Lu, Rapid solidification and liquid-phase separation of undercooled CoCrCuFexNi high-entropy alloys, Intermetallics 72 (2016) 44–52, https://doi.org/10.1016/j.intermet.2016.01.008.
[22] W.L. Wang, L. Hu, S.B. Luo, L.J. Meng, D.L. Geng, B. Wei, Liquid phase separation and rapid dendritic growth of high-entropy CoCrCuFeNi alloy, Intermetallics 77 (2016) 41–45.
[23] J. Valloton, D.M. Herlach, H. Henein, D. Sediako, Microstructural quantification of rapidly solidified undercooled D2 tool steel, Metall. Mater. Trans. A Phys. Metall. Mater. Sci. 48 (2017) 4735–4743, https://doi.org/10.1007/s11661-017-4249-9.
[24] J.F. Li, W.Q. Jie, G.C. Yang, Y.H. Zhou, Solidification structure formation in undercooled Fe-Ni alloy, Acta Mater. 50 (2002) 1797–1807, https://doi.org/10.1016/S1359-6454(02)00032-0.
[25] J.F. Li, Y.C. Liu, Y.L. Lu, G.C. Yang, Y.H. Zhou, Structural evolution of undercooled Ni-Cu alloys, J. Cryst. Growth 192 (1998) 462–470, https://doi.org/10.1016/S0022-0248(98)00399-6.
[26] A. Munitz, R. Abbaschian, Liquid separation in Cu – Co and Cu – Co – Fe alloys solidified at high cooling rates, Mater. Sci. 33 (1998) 3639–3649, https://doi.org/10.1023/A:1004663530929.
[27] A. Munitz, R. Abbaschian, Two-melt separation in supercooled Cu-Co alloys solidifying in a drop-tube, J. Mater. Sci. 26 (1991) 6458–6466, https://doi.org/10.1007/BF00551897.
[28] A.R. Miedema, F.R. de Boer, R. Boom, Model predictions for the enthalpy of formation of transition metal alloys, Calphad 1 (1977) 341–359, https://doi.org/10.1016/0364-5916(77)90011-6.
[29] T. Zhang, F. Liu, H.F. Wang, G.C. Yang, Grain refinement in highly undercooled solidification of Ni85Cu15alloy melt: direct evidence for recrystallization mechanism, Scripta Mater. 63 (2010) 43–46, https://doi.org/10.1016/j.scriptamat.2010.03.006.
[30] O. Funke, G. Phanikumar, P.K. Galenko, L. Chernova, S. Reutzel, M. Kolbe, et al., Dendrite growth velocity in levitated undercooled nickel melts, J. Cryst. Growth 297 (2006) 211–222, https://doi.org/10.1016/j.jcrysgro.2006.08.045.
[31] K. Eckler, D.M. Herlach, M.J. Aziz, Search for a solute-drag effect in dendritic solidification, Acta Metall. Mater. 42 (1994) 975–979, https://doi.org/10.1016/0956-7151(94)90291-7.
[32] G. Phanikumar, K. Biswas, O. Funke, D. Holland-Moritz, D.M. Herlach, K. Chattopadhyay, Solidification of undercooled peritectic Fe-Ge alloy, Acta Mater. 53 (2005) 3591–3600, https://doi.org/10.1016/j.actamat.2005.03.053.
[33] M. Hillert, B. Sundman, A solute-drag treatment of the transition from diffusion-controlled to diffusionless solidification, Acta Metall. 25 (1977) 11–18, https://doi.org/10.1016/0001-6160(77)90240-1.
[34] J.A. Kittl, M.J. Aziz, D.P. Brunco, M.O. Thompson, Nonequilibrium partitioning during rapid solidification of Si-As alloys, J. Cryst. Growth 148 (1995) 172–182.